MICROCOPY RESOLUTION TEST CHART

NATIONAL BUREAU OF STANDARDS-1963-A

AD-A195 226

FILE COPY ②

REPORT DOCUMENTATION PAGE

1a. REPORT SECURITY CLASSIFICATION UNCLASSIFIED	1b. RESTRICTIVE MARKINGS
2a. SECURITY CLASSIFICATION AUTHORITY	3. DISTRIBUTION/AVAILABILITY OF REPORT
2b. DECLASSIFICATION/DOWNGRADING SCHEDULE	Approved for public release; distribution unlimited.

4. PERFORMING ORGANIZATION REPORT NUMBER(S)	5. MONITORING ORGANIZATION REPORT NUMBER(S)
	AFOSR·TR· 88-0545

6a. NAME OF PERFORMING ORGANIZATION	6b. OFFICE SYMBOL (If applicable)	7a. NAME OF MONITORING ORGANIZATION
Polytechnic University		AFOSR/NE

6c. ADDRESS (City, State and ZIP Code)	7b. ADDRESS (City, State and ZIP Code)
333 Jay Street Brooklyn, NY 11201	Bldg 410 Bolling AFB, DC 20332-6448

8a. NAME OF FUNDING/SPONSORING ORGANIZATION	8b. OFFICE SYMBOL (If applicable)	9. PROCUREMENT INSTRUMENT IDENTIFICATION NUMBER
Same as 7a		AFOSR-86-0318

8c. ADDRESS (City, State and ZIP Code)	10. SOURCE OF FUNDING NOS.			
	PROGRAM ELEMENT NO.	PROJECT NO.	TASK NO.	WORK UNIT NO.
Same as 7b	61102F	2306	A3	

11. TITLE (Include Security Classification)
In Situ Fault Detection by the Hybrid Ray-Mode Method

12. PERSONAL AUTHOR(S)
Professor Felsen, L. B.

13a. TYPE OF REPORT	13b. TIME COVERED	14. DATE OF REPORT (Yr., Mo., Day)	15. PAGE COUNT
Annual Report	FROM 1 Mar 87 TO 29 Feb	88	

16. SUPPLEMENTARY NOTATION

17. COSATI CODES			18. SUBJECT TERMS (Continue on reverse if necessary and identify by block number)
FIELD	GROUP	SUB. GR.	

19. ABSTRACT (Continue on reverse if necessary and identify by block number)
The objective of this research effort has been to develop algorithms for in situ location, by ultrasound, of flaws in plates or laminated layered materials. Achieving this objective requires detailed knowledge of the excitation, propagation, scattering and detection of high frequency sound waves in the flawed environment. Based on an understanding of these fundamental wave phenomena, one may then atttempt to construct analytical models with accompanying algorithms, so as to parametrize the NDE problem in terms of "good observables".

DTIC ELECTE MAY 1 9 1988 E

20. DISTRIBUTION/AVAILABILITY OF ABSTRACT	21. ABSTRACT SECURITY CLASSIFICATION
UNCLASSIFIED/UNLIMITED ☐ SAME AS RPT. ☐ DTIC USERS ☐	UNCLASSIFIED

22a. NAME OF RESPONSIBLE INDIVIDUAL	22b. TELEPHONE NUMBER (Include Area Code)	22c. OFFICE SYMBOL
WEINSTOCK	202-767-4933	NE

DD FORM 1473, 83 APR   EDITION OF 1 JAN 73 IS OBSOLETE.

SECURITY CLASSIFICATION OF THIS PAGE

Polytechnic University

Annual Technical Report - 1 Mar. 87 - 29 Feb. 88

AFOSR Grant No. 86-0318

"IN SITU FAULT DETECTION BY THE HYBRID

RAY MODE METHOD"

L. B. Felsen
Principal Investigator
Phone: (516)755-4203

J. M. Klosner
Co-Principal Investigator
Phone: (516)755-4210

Accession For	
NTIS GRA&I	☒
DTIC TAB	☐
Unannounced	☐
Justification	
By	
Distribution/	
Availability Codes	
Dist	Avail and/or Special
A-1	

DTIC COPY INSPECTED 6

"IN SITU FAULT DETECTION BY THE HYBRID

RAY MODE METHOD"

Polytechnic University

AFOSR Grant No. 86-0318

Annual Technical Report - 1 Mar. 87 - 29 Feb. 88

I. Background
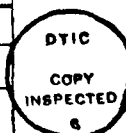
The objective of this research effort has been to develop
algorithms for in situ location, by ultrasound, of flaws in
plates or laminated layered materials. Achieving this objec-
tive requires detailed knowledge of the excitation, propaga-
tion, scattering and detection of high frequency sound waves
in the flawed environment. Based on an understanding of these
fundamental wave phenomena, one may then attempt to construct
analytical models with accompanying algorithms, so as to par-
ametrize the NDE problem in terms of "good observables". Dur-
ing the reporting period, carefully selected prototype problems
have been investigated to determine "good observables" for par-
ticular flawed environments.

II. Accomplishments

A. Gaussian Beam Excitation of a Solid Plate

Near completion is a study directed toward clarifying wave
phenomena generated by a two-dimensional Gaussian beam input in
a layered elastic solid as exemplified (though the general multi-
layer theory has been developed) by an aluminum plate in vacuum
[1]. The Gaussian input has been chosen because a) Gaussians are
good models for smoothly tapered outputs from actual transducers,
and b) they can be used as discrete basis elements on a (config-

uration)- (spatial wavenumber) phase space lattice to model rigorously *any* transducer output [2]. The Gaussian input is analyzed via the complex source point (CSP) method, by which beam excitation solutions in any (here, the layered) environment are obtained from line or point source excitation solutions in that environment by assigning complex values to the source coordinate location [3]. This avoids the need for spatial spectral decomposition of the beam field, as is customary. Previous applications of the CSP method, which requires careful study of the analytic continuation to the complex source domain, have not dealt with elastic layers. Some difficulties encountered in this process are still under investigation, but in the present application to a compressional (P) beam input, they were de-emphasized and do not affect the validity of the results. Extensive numerical computations have been performed to chart the evolution of the P-beam input as it interacts with the plate boundaries and undergoes P-SV coupling at each reflection. The resulting displacement profiles reveal clearly the beam-like character near the source, the deterioration of the successively reflected beam due to P-SV coupling at the boundaries, and the eventual evolution of oscillatory mode-like patterns. The results strongly suggest that a hybrid beam-mode format is worthy of consideration because the physical observables appear beam-like in certain parametric domains and mode-like in others.

B. Gaussian Beam Excitation of a Flawed Solid Plate

In conjunction with the investigation of the unflawed plate (Section IIA) has been a study aimed at determining "good parametrizations" of observables when two-dimensional Gaussian P-

beam excitation of a perfectly bounded layered elastic plate (which appears like a single-layer thick plate) encounters a transversely thin region with a weak bond imperfection. The flaw is assumed to give rise to reduced shear resistance. The problem has been treated by considering first the fields excited by the input beam in the unflawed environment, and then allowing these fields to interact with the flaw; the scattered fields produced thereby are monitored at the receiver on the surface. As before, the input beam was modeled compactly by a line source at a complex coordinate location (complex source point (CSP) method [3]), which permits the beam input response to be computed from the line source input response by analytic continuation of the source coordinates into the complex domain.

The results from the unflawed problem (Section IIA) [1] provided the input for the flawed configuration. Since the adhesive layer was assumed to be thin in comparison to the compressinal and shear wavelengths, the bond can be represented by distributed shear springs. Limiting the model to weak imperfections permits the equivalent surface fields induced on the flaw to be approximated by the incident field as modified by the stiffness profile (Born Approximation). The scattering produced in the plate by the resulting equivalent source distribution was evaluated by surface integration over the flaw contour, using the line force plate Green's function as a kernel. Primary attention was placed on determining the physical observables (the horizontal and vertical displacements) at the detector on the plate boundary. The parametrization seeks to connect these observables with presence, location, and physical constitution of the flawed region.

In the studies so far, the incident beam interacts with the flaw before being diffused by multiple reflections. This makes the beam perturbed by the flaw a "good observable" and suggests a beam oriented parametrization. In this endeavor, a choice of input conditions that combines beam resolution with strong shear excitation at the site of the flaw plays a critical role. Numerical results show that a good parametrization can be achieved in this way. Some indications have been given on how to make the inverse connection between surface displacements and flaw identification, but work on this aspect is still in progress.

References

[1] Lu, I.T., Felsen, L.B., and Klosner, J.M., "Observables Due to Beam-To-Mode Conversion of a High Frequency Gaussian P-Wave Input in an Aluminum Plate in Vacuum", to be presented at the Symposium on New Directions in the Ultrasonic NDE of Advanced Materials, 1988 ASME Winter Meeting.

[2] Maciel, J.J. and Felsen, L.B., "Systematic Study of Fields Due to Extended Apertures by Gaussian Beam Discretization", to be published in IEEE Transactions on Antennas and Propagation.

[3] Felsen, L.B., "Geometrical Theory of Diffraction, Evanescent Waves, Complex Rays and Gaussian Beams", Geophys. J. Roy, Astron. Soc., 79, 77-88 (1984).

III. Publications and Meeting Papers

The accomplishments in Section II have been, and are being, documented in manuscripts and presented at technical conferences. Manuscripts and meeting paper abstracts are attached.

A. Publications

[1] Lu, I.T., Felsen, L.B. and Klosner, J.M., "Beam-To-Mode Conversion of a High Frequency Gaussian P-Wave Input in an Elastic Plate Embedded in Vacuum", to be published in Review of Progress in Quantitative Nondestructive Evaluation, Vol. 6, 1987. Copy attached as Appendix A.

[2] Lu, I.T., Felsen, L.B., and Klosner, J.M., "Observables Due to Beam-To-Mode Conversion of a High Frequency Gaussian P-Wave Input in an Aluminum Plate in Vacuum", to be published in Proceedings of the Symposium on New Directions in the Ultrasonic NDE of Advanced Materials. In preparation.

[3] Lu, I.T., Felsen, L.B., Klosner, J.M. and Gabay, C., "Beam and Mode Analysis of Weak Bonding Flaws in a Layered Aluminum Plate", to be published in the Proc. IUTAM-IUPAP Symp. on Elastic Wave Propagation, held in Galway, Ireland, 20-25 March 1988. Copy attached as Appendix B.

B. Meeting Papers

[1] Lu, I.T., Felsen, L.B. and Klosner, J.M., "Beam-To-Mode Conversion of a High Frequency Gaussian P-Wave Input in an Elastic Plate Embedded in Vacuum", presented at Fourteenth Annual Review of Progress in Quantitative NDE, Williamsburg, Va., 1987.

[2] Lu, I.T., Felsen, L.B. and Klosner, J.M., "Beam-to-Mode Conversion of a High Frequency Gaussian P-Wave Input in an Elastic Plate Embedded in Vacuum", presented at the 114th Meeting of the Acoust. Soc. Amer., Miami, Fla., 16-20 November 1987.

[3] Lu, I.T., Felsen, L.B., Klosner, J.M. and Gabay, C., "Beam and Mode Analysis of Weak Bonding Flaws in a Layered Aluminum Plate", presented at the IUTAM-IUPAP Symp. on Elastic Wave Propagation, Galway, Ireland, 20-25 March 1988.

[4] Lu, I.T., Felsen, L.B., and Klosner, J.M., "Observables Due to Beam-To-Mode Conversion of a High Frequency Gaussian P-Wave Input in an Aluminum Plate in Vacuum", to be presented at the Symposium on New Directions in the Ultrasonic NDE of Advanced Materials, 1988 ASME Winter Meeting.

IV. Personnel

The following personnel have been associated with this Grant during the reporting period:

* Dr. Leopold B. Felsen, Institute Professor, Principal Investigator

** Dr. Jerome M. Klosner, Professor, Co-Principal Investigator

* Dr. I. T. Lu, Assistant Professor

** C. Gabay, Ph.D. Candidate

* Dept. of Electrical Engineering and Computer Science

** Dept. of Mechanical and Industrial Engineering

BEAM-TO-MODE CONVERSION OF A HIGH FREQUENCY GAUSSIAN P-WAVE

INPUT IN AN ELASTIC PLATE EMBEDDED IN VACUUM

I. T. Lu, L. B. Felsen and J. M. Klosner
Polytechnic University
Route 110
Farmingdale, New York 11735

INTRODUCTION

Identification of flaws in solid or laminated layered materials by ultrasound requires detailed knowledge of the excitation, propagation, scattering and detection of high frequency sound waves in the flawed environment. An overall approach to this problem, whereby one seeks to parametrize all relevant wave phenomenon in terms of "good observables", will be discussed elsewhere. Here, we report on the first phase dealing with excitation. In modeling actual or induced source distributions, we assign a special role to Gaussian inputs because a) Gaussians individually can simulate certain smoothly tapered distributions, and b) a superposition of Gaussians on a self-consistent (configuration - wavenumber) space lattice can represent any prescribed distribution. To generate the Gaussian beams that propagate the Gaussian input into the environment, we utilize the complex source point (CSP) method because it avoids the plane wave spectral analysis and synthesis required in the conventional approach. By the CSP method, Green's functions for beam sources are derived directly from Green's functions for line or point sources by analytic continuation to complex source locations. While the CSP method has been applied previously to beam propagation and diffraction in fluid media [1-7], and to studying such phenomena in semi-infinite solids [8-9], our concern here with layered elastic media necessitates attacking new problems in the rigorous analytic continuation process that have not been encountered in earlier studies. These problems are highlighted here, but their resolution is still in progress and will be reported separately. In the results cited below, excitation conditions have been chosen so as to de-emphasize the sources of difficulty.

The problem posed in the present investigation is the mechanism of conversion of a well-collimated input beam in a layered elastic medium into the spectrum of guided modes, favored among which is a particular mode, one of whose congruences is aligned with the incidence beam angle. The transitional phase is of interest because, for optimum versatility, it may be desirable to choose operating conditions that accommodate in a continuous manner beam-type, mode-type, or combinations of input field interactions with a fault zone. Although the formal theory has been constructed for the general case, we have restricted our initial numerical implementation to a simple test case: a P-wave beam source located in an elastic plate, which is embedded in vacuum. Results have been generated via the ray-tracing and normal mode expansion algorithms, published previously [10] but generalized here by the CSP substitution. Some of the difficulties encountered in this generalization are summarized in the following section and typical numerical results are shown and discussed. The data clearly reveals the influence of P-SV boundary coupling on the beam-to-mode conversion process.

COMPLEX-SOURCE POINT FORMULATION

To convert the wave fields due to the conventional P-wave isotropic line source (Fig. 1a) into wave fields corresponding to excitation by a P-wave Gaussian beam source (Fig. 1b), we shall employ the complex source point technique mentioned earlier. This requires analytic continuation of all wavefield expressions from the real source coordinates (x', z') to the complex source coordinates

$$\tilde{x}' = x' + ib \cos \alpha \, , \, \tilde{z}' = z' + i b \sin \alpha \tag{1}$$

where (x′, z′) now locates t̲ ̲center of the beam waist, b is a beam̲ ̲Jth parameter, and α is the angle between the beam axis and the positive x-axis (see Fig. 1b and Refs. [1-9]). While the analytic extension guarantees formally that the resulting P and SV potentials satisfy the appropriate wave equations and boundary conditions, the validity of a particular wavefield representation must be verified in each case; i.e., the

representation obtained on replacing (x′, z′) by (x̃′, z̃′) must remain convergent. It turns out that various alternative representations require different continuation strategies.

When the wavefield representation is in the form of a spectral integral over the spatial wavenumber k corresponding to the x-coordinate, the analytic extension can be carried out systematically by contour deformation, if required. Because the integrand depends analytically on x′ and z′, convergence can be tested continuously as x′ and z′ are made complex. If, for certain parameter ranges, convergence at |k| →∞ turns out to be violated on the original contour, that contour can be deformed into appropriate regions of the complex k plane wherein convergence is retained. When the representation is in the form of a series like the normal mode or the hybrid ray-mode expansion [10], direct

(x̃′ z̃′) substitution may cause convergence problems due to exponentially growing factors in the series elements. Contour deformation is now not an immediately available option. We shall report elsewhere on how to proceed in this case. For presentation here, we have chosen the beam parameters so that these difficulties can be avoided. We have so far dealt with the analytically extended ray and normal mode representations. Although both formulations must (and do) generate the same result, the ray formulation allows beam tracking through an increasing number of reflections at the boundaries while the mode representation highlights the fully excited guiding phenomena.

In tracking the beam integrals [6], it is desirable to switch from the global (x,z) coordinates to the local coordinates defined with respect to the axes of the individual beams (see Fig. 1b). This stabilizes the analytic continuation by avoiding oblique spectra with respect to the beam axes at beam propagation angles approaching the x-direction and de-emphasizing problems attributable to boundary reflections of evanescent spectra. To illustrate these aspects, we consider first the incident P-beam potential, which behaves as though it propagates in unbounded space. From Eq. (2) in [6] and Eq. (1), it is given in the global (x,z) system by

$$\Phi = - \frac{1}{4\pi i} \int_{-\infty}^{\infty} \frac{1}{\kappa_p} \exp \left\{ i[\kappa_p(z-z'-ib \sin \alpha)+k(x-x'-ib \cos \alpha)] \right\} dk \qquad (2)$$

where $\kappa_p = \sqrt{k_p^2-k^2}$, $k_p=\omega/v_p$, v_p is the P-wave propagation speed, and ω is the radian frequency. The integration path avoids the branch point singularities at $(+k_p)$ and $(-k_p)$ by indentations into the fourth and second quadrants, respectively, of the complex k-plane. The condition

$$z - z' > b \cos \alpha \qquad (3)$$

guarantees convergence of the integrand at k → ±∞. In fact, the integrand decays in the intervals from ±k_p to ±∞, as can be verified by observing that for k>k_p and when Eq. (3) holds, the real part of the phase in Eq. (2) has a negative derivative with respect to k. This establishes the existence of an evanescent spectrum. The SV-beam potential generated by reflection of this incident beam from the solid-free space interface is, in the global (x,z) system [6],

$$\Psi = - \frac{1}{4\pi i} \int_{-\infty}^{\infty} \frac{\Gamma_{sp}}{\kappa_p} \exp \left\{ i[\kappa_p(z'+ib \sin \alpha)+\kappa_s z+k(x-x'-ib \cos \alpha)] \right\} dk \qquad (4)$$

where Γ_{sp} accounts for P-S coupling at the boundary, $\kappa_s = \sqrt{k_s^2-k^2}$, $k_s = \omega/v_s$, and v_s is the S-wave propagation speed. The condition

- 2 -

$$(z'+z) > b \cos \alpha \tag{5}$$

again ensures the convergence of the integrand at $k \to \pm\infty$. Note, however, that the real part A of the phase in Eq. (4) is

$$A = -\sqrt{k^2 - k_p^2}\, z' + kb \cos \alpha \quad \text{when } k_s > k > k_p \tag{6}$$

If

$$dA/dk \Big|_{k=k_s} = \frac{-k_s}{\sqrt{k_s^2 - k_p^2}}\, z' + b \cos \alpha > 0 \tag{7}$$

the spectral amplitudes will <u>grow</u> in the interval $[k_p, k_s]$, which behavior is computationally inconvenient, and physically unnatural because the source beam spectrum in that interval is decaying. The anomaly is avoided by choice of local coordinates and corresponding spectral decomposition tied to the incident beam so that the beam angle in this local system equals $\alpha = \pi/2$; the local coordinate system is updated for each reflection.

When the complex source coordinate substitution is performed on the modal sum, the nonphysical anomaly attributed to the $k_p < k < k_s$ domain is not avoided so easily. Pending further investigation, we have for the present simply ignored the modes with modal eigenvalues $k_m > k_p$ beca se their excitation strength by the specified P-wave source is minimal. Numerical comparisons with fields computed by the beam tracking algorithm have confirmed the validity of this assumption.

A NUMERICAL EXAMPLE

The mechanism of conversion of an initially well collimated incident beam in an elastic plate into a spectrum of modes centered around the one "best matched" to the incident spectrum is illustrated by a numerical example. The parameters used in the calculations pertain to an (aluminum) plate (see Fig. 1a):

$$v_p = 2.36 \times 10^5 \text{ in./sec.}, \quad v_s = 1.209 \times 10^5 \text{ in./sec.},$$

$$\rho = 2.53 \times 10^{-4} \text{ lb.-sec.}^2/\text{in.}^4, \quad a = 0.1 \text{ in.} \tag{8}$$

The 60 MHz P-source beam waist has been placed at $z' = 0.04$ in., $x' = 0.0$ in., with beam width parameter $b = 0.1$ in. The beam axis inclination $\alpha = 0.548$ rad. (see Fig. 1b) lines up with the upward P-plane wave congruence of one of the guided modes. The axes of the incident P-beam, the reflected P-beam and the converted SV-beams are indicated in the figure. Fig. 2 shows the magnitude of the resulting P and SV potentials Φ (dashed) and Ψ (solid), respectively, plotted in cross sections at the axial distances $x = 0.05, 0.08, 0.11, 0.14, 0.17, 0.23$ inches (see Fig. 1b). The potentials have been calculated by the normal mode expansion in [10] and by the ray series in [10]. After employing the complex source coordinates in Eq. (1), both procedures yield the same numerical values. In the normal mode expansion, as mentioned before, we have retained only those modes (64 in this example) with $k_m < k_p$ because physical considerations dictate that the incident P beam couples very weakly to the evanescent P spectra contained in modes with $k_m > k_p$.

The beam-to-mode conversion process is well illustrated by the results. In the cross section at $x = 0.05$ in., the incident P beam is still far enough from the upper boundary to render the effect of that boundary small. Accordingly, the P potential retains its essentially Gaussian shape (note that the $x = $ constant planes do not conform with the natural beam-centered coordinate planes perpendicular to the beam axes). The off-axis spectra in the Gaussian tail, which do interact with the boundary, produce the very weak decaying P-SV reflection and the P-P reflection ripple near the top of the P data. In the next observation plane at 0.08 in., the incident beam axis has approached the upper boundary sufficiently closely to cause more substantial P-P reflection and P-SV

conversion of the off-axis ctra. Interference between the incide nd reflected P spectra is evident by the more substantial ripple, and the converted .. spectra, though weak at the bottom, extend over the entire cross section. The incident beam axis strikes the top boundary before the next observation plane at $x = 0.11$ in., which therefore contains the traces of both the reflected P and SV beam axes. Strong interference between the P and P-P process near the top boundary is evident, but one may also discern a P potential rise near the bottom, which is due to P-SV-P conversion. The SV spectra near the bottom boundary are now strong enough to cause such conversion, as well as the SV-SV reflection ripple in the solid curve, whereas the bulk of the SV reflected beam has moved from the top toward the plate center. It may be noted that the maximum of the wide SV reflected beam is shifted away from the SV beam axis intercept with the observation plane. This shift is due in part to apparent asymmetries introduced by the substantial deviation of the x = const. plane from the "natural" coordinate plane transverse to the beam axis, and also to the lateral shift of the reflected SV beam axis on the top boundary which is known to accompany the P-SV conversion. These phenomena are further enhanced at $x = 0.14$ in., and also at $x = 0.17$ in. where substantial reflection and P conversion of the downgoing SV beam at the bottom make their contribution. Clearly, individual beams (certainly for SV waves but also for P waves) are now difficult to resolve, and the potentials begin to stabilize toward oscillatory patterns with fixed periodicity. These periodicities turn out to be essentially those found in the guided mode whose upgoing plane wave P spectra line up most closely (in our case, exactly) with the dominant wave spectra of the incident P beam (i.e., with the beam axis if the incident beam is well collimated). The SV periodicity pattern is already well established at $x = 0.17$ in. because the SV beams with their steeper propagation angles have had an opportunity to interact with both the top and bottom surfaces of the plate. For the P patterns, larger x values are required before the analogous interactions and consequent periodicity stabilizations occur; we have verified that $x = 0.23$ in. is adequate (see Fig. 2). Other more extensive calculations are in progress and will be reported elsewhere.

DISCUSSION

In this paper, we have explored the mechanism by which an incident well collimated beam excites the spectrum of guided modes that can be supported in a layered structure. For simplicity, we have chosen a single elastic plate embedded in vacuum, but other models, with exterior fluid loading, are already under consideration. Results for the P and SV potentials in successive cross sections have been computed numerically by the beam tracking algorithm and by normal mode expansion. Both being formally exact, they are expected to (and they do) furnish the same numerical data. Concerning the form of the result, the field in initial cross sections is beam shaped, reproducing essentially the incident beam in unbounded space, before it reaches one of the boundaries. This suggests that the wave fields in the plate should be calculated in this parameter regime by beam functions. Expansion in terms of the spectrum of guided modes in the plate is equally valid, but many modes are required to synthesize the Gaussian beam profile. Thus, guided modes are phenomenologically unsuited and furnish poor observables here, whereas beams furnish good observables. After the beam has interacted with one of the boundaries, the resulting interference and conversion phenomena blur the originally clean beam profile, and after successive reflections, any resemblance to beams has disappeared altogether. The wave pattern in the cross section becomes oscillatory, thereby implying that the good observables are now the guided modes. This suggests use of our beam-generated self-consistent hybrid ray-mode algorithm [10], which can be structured so that it encompasses automatically the transition from one good observable parametrization to the other. This aspect is now under investigation.

One interesting observation has already emerged from these numerical results. It was noted earlier that a few reflections between the plate boundaries suffice to diffuse the profile of an initially well collimated beam into a cross sectional standing wave pattern. The periodicity of this pattern is well reproduced by that of the guided mode, one of whose constituent plane wave congruences is closely aligned with the dominant wave spectra that propagate along the axis of the incident beam. Thus, the total field

stabilizes rather quickly to J the periodicity pattern of the mode   ored by the incident beam. However, that mode is not excited in pure form as ᴄ .denced by the nonuniform amplitude profile of the total field. Therefore, the function of modes with other periodicities seems to be primarily to adjust the amplitudes in the oscillatory pattern to their proper values. The close matching of the total field periodicities with those of the favored mode is important because good prediction of null locations is required for wavefield interaction with structural faults. Further study of this phenomenon is intended to ascertain whether these observations apply also under more general conditions.

ACKNOWLEDGEMENT

REFERENCES

1. L. B. Felsen, Philips Res. Rep, 30, 187-195 (1975).

2. A. C. Green, H. L. Bertoni and L. B. Felsen, J. Opt. Soc. Am., 69, 11 (1979).

3. L. B. Felsen, Geophys. J. R. astr. Soc., 79, 77-88 (1984).

4. X. J. Gao and L. B. Felsen, IEEE Trans. Antennas Propag., AP-33, 963-975 (1985).

5. Y. Z. Ruan and L. B. Felsen, J. Opt. Soc. Am., A, 566-579 (1986).

6. I. T. Lu, L. B. Felsen, Y. Z. Ruan and Z. L. Zhang, IEEE Trans. Antennas Propag., AP-35, 809-817 (1987).

7. I. T. Lu, L. B. Felsen and Y. Z. Ruan, Geophys. J. R. astr. Soc., 89, 915-932 (1987).

8. J. Harris and J. Pott, J. Acoust. Soc. Am. 78(3), 1072-1080 (1985).

9. B. S. White, A. Norris, A. Rayliss and R. Burridge, Geophys. J. R. astr. Soc., 89, 579-636 (1987).

10. I. T. Lu and L. B. Felsen, J. Acoust. Soc. Am., 78, 701-714 (1985).
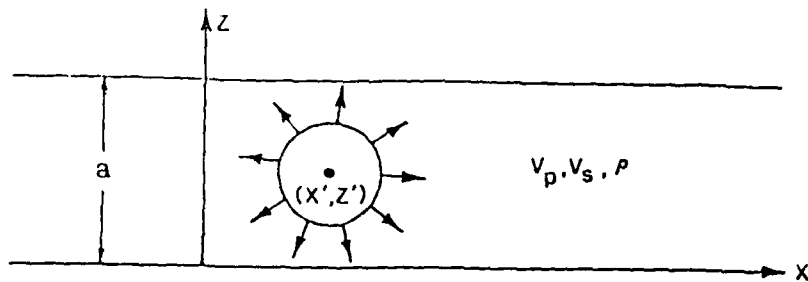
(a)   real source coordinates (x′, z′) (P-wave isotropic line source).
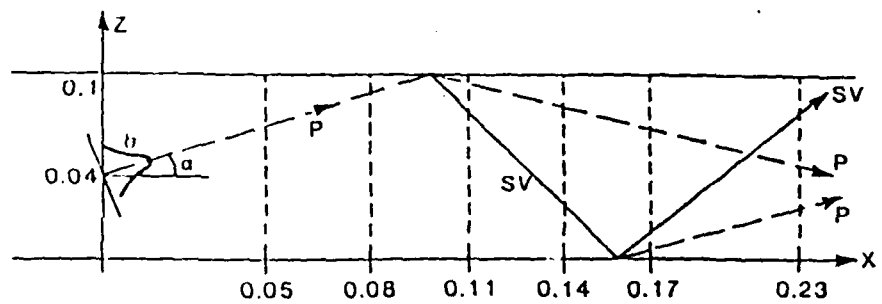
(b)   complex source coordinates ($\tilde{x}′$, $\tilde{z}′$) (P-wave beam source). The beam parameter b
in (1) is related to the (1/e) beam width w_e at the waist, $w_e = (2b/k_p)^{1/2}$. Also
shown on this figure are the axes of the incident and reflected P-beams (dashed
lines), and of the coupled SV-beams (solid lines), and their relationship to the
cross sections in Fig. 2.

Fig. 1.   Elastic plate with thickness a, characterized by wave velocities v_p, v_s and by
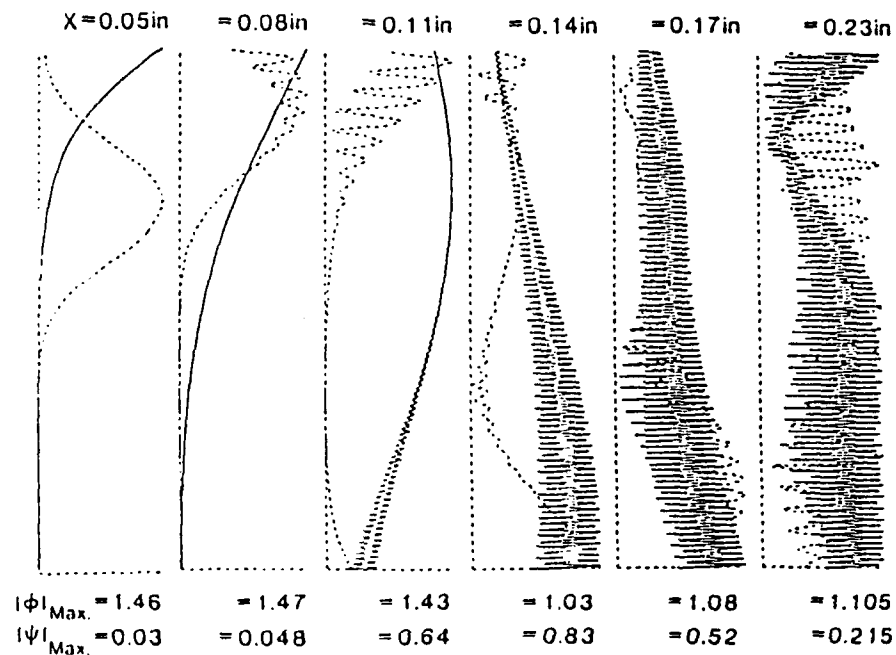density ρ.

Fig. 2.   Amplitude profiles of the P-wave potential Φ (dashed) and the SV-wave
potential Ψ (solid) due to a P-beam input, observed at successive plate cross
sections in the interval from x = 0.05 in. to x = 0.23 in. The plate parameters
are in (8) and the frequency is 60 MHz. The beam parameters are: $x' = 0$, $z' =$
0.04 in., $\alpha = 0.548$, b = 0.1 in. The vertical axis measures the cross sectional
coordinate z. The horizontal axis measures $|\Phi|$ and $|\Psi|$, respectively, on
different scales, with the maximum in each wave denoted by the number
listed. This figure should be viewed together with Fig. 1b, which shows the
disposition of the incident and reflected beam axis.

BEAM AND MODE ANALYSIS OF WEAK BONDING FLAWS IN A LAYERED ALUMINUM PLATE

by

I.T. Lu,* L.B. Felsen,* J.M. Klosner** and C. Gabay**
*Department of Electrical Engineering and Computer Science
Weber Research Institute

and

**Mechanical and Aerospace Engineering Department
Polytechnic University, Farmingdale, NY 11735 USA

Location and identification of faults in multilayer elastic materials by ultrasound is aided by a physically based parametrization of the input, scattered and detected fields. When the transducer input is beam-shaped, the beam-to-mode conversion in the unflawed layered environment suggests a "good" parametrization in terms of a self-consistent hybrid beam-mode format. The scattered field produced by interaction of this beam-mode field with a fault zone should then be parametrized in a similar manner. This strategy guides the present investigation of a weak bonding flaw in a multilayer aluminum plate. The horizontal and vertical displacements excited by a high frequency two-dimensional dilatational (P) Gaussian input beam have previously been tracked through successive cross sections in the perfectly bonded material. The resulting displacement profiles reveal clearly the beam-like character near the source, the deterioration of the successively reflected beam due to P-SV coupling at the boundaries, and the eventual evolution of oscillatory mode-like patterns. This input is now allowed to interact with an elongated weak bond zone. The induced equivalent forcing terms are modeled in the Born approximation, and the scattered field is evaluated accordingly. Depending on the flaw size, its location relative to the input and output transducers, and other variables, the detected response at the plate surface may contain beam-like or mode-like features. The beam-like phenomena are explored here with a view toward finding conditions through which the physical observables that should facilitate flaw location and identification are enhanced. Although, for convenience, the numerical data have been generated by normal mode summation, the results reveal clearly that the hybrid beam-mode format, to be developed next, furnishes the proper parametrization.

1. INTRODUCTION

Analytical modeling of flaw identification in a layered composite through response to an ultrasonic beam input poses a problem of substantial complexity. A good identification scheme must rely on a good parametrization of the propagation and scattering process in terms of physical observables. Translating such observables into analytic form is usually done best by selecting coordinates that are well matched to the phenomenology. This is easily accomplished when considering the input beam, the flaw induced scattering, and the layered environment in isolation but it is far less transparent when all of these constituents interact: the beam coordinates are generally not matched to those of the flaw nor to those of the layers. Thus, analytical basis ele-

ments that describe com-actly the wave phenomena associated with one of the consti-tuents are likely to be awkward and less physical for the other constituents. One attempt to cope with these difficulties is via self-consistent hybrid combinations of different basis elements, chosen so as to model the various observables in those parameter ranges where they are most pronounced.

In a previous and the present investigation, an effort has been made to address these concerns systematically. The overall problem has been decomposed by considering first the fields excited by the input beam in the unflawed environment, to be followed by the interaction of these fields with the flaw, and the consequent scattered fields produced thereby at the receiver. For simplicity, the problem is taken to be two-dimensional, and the unflawed material is a perfectly bonded layered aluminum plate (which therefore acts like a single thick layer) in vacuum. The input beam is assumed to be compressional (P-wave) and to have a Gaussian profile so that it can be modeled compactly by a line source at a complex coordinate location (complex source point (CSP) method) [1]. This permits the beam input response to be computed from the line force input response by analytic continuation of the source coordinates into the complex domain. Depending on whether the observer is near, or far from, the source region, the field in the plate has a beam-like or mode-like character, undergo-ing rapid conversion from the former to the latter due to multiple reflections, with consequent compressional-shear (P-SV) coupling, at the plate boundaries. A hybrid ray-mode form can describe this phenomenology. This first (unflawed) phase of the problem has already been treated in detail [2], and the results from that investigation provide the input for the flawed environment here.

To test the proposed problem strategy without undue analytic complication, an imper-fect bond of finite extent aligned parallel to the plate boundaries has been postulated. The imperfection pertains only to reduced shear resistance, and thus, since the adhesive layer is thin in comparison to the wavelengths, the bond can be represented by distributed shear springs. For weak imperfections, the equivalent surface fields induced on the flaw can be approximated by the incident field as modified by the stiffness profile (Born approximation); because the flaw responds to tangential shear but not to compression, the incident field at the flaw site should have a strong longitu-dinal shear component. The scattering produced in the plate by the resulting equivalent source distribution can be evaluated by surface integration over the flaw contour, using the line force plate Green's function. The detector is assumed to be located on the plate boundary; therefore, primary attention is placed on determining the physical observables (i.e., the horizontal and vertical displacements) there.

The presentation below begins with a summary description of beam excited fields that have favorable properties for interaction with the flaw in the thick plate, and of "good" parametrizations of these fields. The surface integral for the scattered field is formu-lated next, with expressions given for the scattering induced displacements on the plate surface. The detection strategy emphasizes beam-like phenomena. Qualitative measures of "good observables" are introduced, which permit drawing inferences about the flaw size and location from the detected data. Each of these phases is accompanied by numerical calculations that demonstrate the detailed field behavior. The paper ends with conclusions based on these results.

2. FORMULATION

2.1 General Concepts

The physical configuration, schematized in Fig. 1, involves a bonded plate of thickness a, constitutive parameters (Lame constants) λ, μ and (density) ρ, with excitation pro-

vided by a two-dimensional ultrasonic harmonic Gaussian P-beam input whose waist is centered at $(x,z) = (0,z')$ and whose inclination with respect to the x-axis is α. A longitudinally oriented thin boundary flaw of length 2ℓ is centered at (x_f, z_f). As noted in Section 1, the bond imperfection is only with respect to its shear resistance, while its full strength is retained in the normal direction. The rigidity of the weakened bond is represented by a distribution of equivalent springs along the flaw contour, the equivalent spring stiffness being defined as

$$K = \tau_{zx}/\Delta u \tag{1}$$

where τ_{zx} is the shearing stress at the joint, and $\Delta u = u^+ - u^-$ denotes the x-displacement jump discontinuity across the bond line.
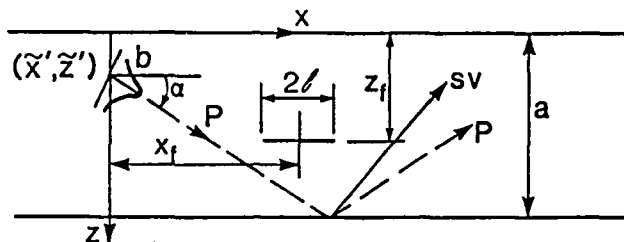

Fig. 1.　　Gaussian P-beam input to elastic plate with bonding flaw of length 2ℓ centered at (x_f, z_f). Incident and reflected P-beam axes (dashed) and reflected SV-beam axis (solid) are included. Numerical data in Figs. 2-6 are for an aluminum plate of thickness $a = 0.3$ in. and bond parameters $x_f = 0.165, 0.135, 0.09, 0.045$, $z_f = 0.15$ in., $2\ell = 0.090$ in. The beam is modeled by the complex source point method, with complex source point location $\tilde{x}' = $ i b cos α, $\tilde{z}' = z' + $ i b sin α, $z' = 0.06$ in., $\alpha = 45°$, $b = 0.3$ in. The corresponding beam waist is $w^e = (2b/k_p)^{1/2} = 0.0335$ in.

The objective is the calculation of the horizontal and vertical displacements $u(x,z)$ and $w(x,z)$, respectively, which constitute the physical observables generated by input forcing functions. Because the problem is composite in the sense described in Section 1, various analytical building blocks are employed to characterize the relevant wave phenomena in a manner amenable to good interpretation. This may require use of different coordinate systems "matched" to particular phenomena (for example, beam centered coordinates instead of the plate coordinates (x,z)). For the force excited displacements, it may be convenient to use the scalar potentials $\hat{\Phi}(x,z)$ and $\hat{\Psi}(x,z)$ pertaining to compressional (P) and vertically polarized (SV) motion, respectively, with propagation speeds $v_p = [(\lambda+\mu)/\rho]^{1/2}$ and $v_s = [\mu/\rho]^{1/2}$. The displacements are derived from the potentials via the differentiations

$$u = \frac{\partial \hat{\Phi}}{\partial x} - \frac{\partial \hat{\Psi}}{\partial z} \quad , \quad w = \frac{\partial \hat{\Phi}}{\partial z} + \frac{\partial \hat{\Psi}}{\partial x} \tag{2}$$

Wave phenomena in the composite environment of Fig. 1 can be synthesized by spectral decomposition and recombination with respect to relevant "preferred" coordinates. For each individual beam, whether incident or multiply reflected, this is best done in the plane perpendicular to the beam axis. For waves "tied" to the plate, the spectral decomposition is along x or z. Decomposition along x organizes the response in terms of a plane wave spectral continuum with horizontal wavenumbers k,

$$\hat{\Lambda}(x,z) = \frac{1}{2\pi} \int_{-\infty}^{\infty} \Lambda(z,\kappa) \, e^{ikx} \, dx \tag{3}$$

where $\Lambda(z,\kappa)$, with $\kappa = \kappa(k)$ representing the vertical wavenumber, is the z-dependent spectral wave amplitude corresponding to the physical quantity $\hat{\Lambda}(x,z)$.

Decomposition along z organizes the response in terms of a discrete spectrum of guided modes with vertical wavenumber κ_m.

$$\hat{A}(x,z) = \sum_m \overline{A}_m(z,\kappa_m)\, e^{ik_m(\kappa_m)x}, \quad x > 0 \tag{4}$$

where m is the mode index and $\overline{A}_m(z,\kappa_m)$ is the mode function. The wavenumbers k and κ are related by the dispersion equations

$$k^2 + \kappa_{p,s}^2 = (\omega/v_{p,s})^2 \quad \text{for P, SV waves,} \tag{5}$$

with $\text{Im}(k \text{ or } \kappa) \geq 0$ to ensure convergence when the wavenumber is nonreal. The continuous wave functions A in (3) or each mode function A_m in (4) can be expressed either in oscillatory form or in terms of upgoing and downgoing plane wave congruences with dependence $\exp(\pm i\kappa z)$ or $\exp(\pm i\kappa_m z)$. The latter, more general, format identifies plane waves as the fundamental spectral building blocks. It should be noted that P-SV coupling at the layer boundaries implies that both wave types have the same horizontal wavenumber k.

The spectral considerations for the beam-excited layer have been described in detail in a separate publication [2]. The phenomenological summary above has been presented to provide justification for subsequently used qualitative estimates that explain the numerically generated displacement observables. For example, the displacements in (2) involve contributions from the differentiated compressional and shear potentials simultaneously, thereby mitigating against the possibility of unscrambling their separate impact in the observed waveforms. However, in either the x-based or z-based spectral domains, it follows for each spectral plane wave element $\sim \exp(i\kappa z + ikx)$ that the derivative operations imply

$$\frac{\partial}{\partial z} \rightarrow i\kappa \quad , \quad \frac{\partial}{\partial x} = ik \tag{6}$$

Thus, depending on the ratio κ/k (i.e., the spectral plane wave propagation angle), one may encounter parameter requirements where either Φ or Ψ predominates. The observed displacements can then be interpreted from the form of the appropriate dominant potential. Conversely, this guideline has been employed by us in the selection of input beams that favor the excitation of strong compression or strong shear.

2.2 Implementation

2.2.1 Beam excited layer without flaw

The solution strategy for charting the evolution of an incident Gaussian P-wave beam in the perfectly bonded layer has been treated analytically and numerically in reference [2]. The beam input has been generated from the line force input by analytic continuation of the source point coordinates from real to complex values, and the potentials, stresses and displacements have been calculated in various vertical cross sections and also along the surface. Guided by the spectral concepts discussed in Section 2.1, it has been possible to explain the observed waveforms in terms of multiply reflected P and SV beams near the input, and in terms of the mode "most favored" by the incident beam in the intermediate and more distant regions. It has also been possible, based on these spectral considerations, to "tune" the input beam parameters so as to generate a desired response, for example, strong horizontal shear in the longitudinal plane that is to contain the flaw. A typical set of response curves is shown in Fig. 2.

With the flaw in place, as shown in Fig. 1, and knowing the incident field at the flaw from the results in Section 2.2.1, one may formulate the scattering problem. In general, this requires solution of a surface integral equation for the unknown induced sources on the flaw. However, in view of the assumed weakness of the imperfection, the induced sources can be approximated by those corresponding to the incident field on the flaw (Born approximation). Accordingly, from (1), the displacement discontinuity across the weakened zone becomes

$$\Delta u^{sc} = \frac{\tau^i_{zx}}{K} \tag{7}$$

where superscripts "i" and "sc" refer to incident and scattered quantities, respectively.

3. SCATTERED FIELDS

The displacements u^{sc} and w^{sc} generated by the initial conditions in (7) can be evaluated by use of Green's function techniques [3],

$$u^{sc}(x,z) = \int_{x_f - \ell}^{x_f + \ell} \Sigma_{zxx}(x',z_f;x,z)\Delta u^{sc}(x',z_f)\ dx'$$

$$w^{sc}(x,z) = \int_{x_f - \ell}^{x_f + \ell} \Sigma_{zxz}(x',z_f;x,z)\Delta u^{sc}(x',z_f)dx' \tag{8}$$

The Green's stress functions Σ_{zxx} and Σ_{zxz} in (8) permit calculation of the shearing stress $\tau_{zx}(x,z_f)$ in a perfectly bonded layer due to a horizontally or vertically polarized input force, respectively. They can be represented in any of the alternative forms discussed in reference [4,5]. In the calculations that follow, the modal expansion form was chosen for convenient reference, but the *interpretation* of the results has been carried out by recourse to spectral concepts tied to "good observables," as described in Section 2.1.

4. NUMERICAL RESULTS

An extensive sequence of numerical calculations has been carried out to gain understanding of the fields generated in the composite geometry of Fig. 1, in particular, the displacements on the upper boundary of the layer, where the detector is assumed to be located. To this end, the displacements generated by the input beam without the flaw, by the scattering in (8), and by the combination of both, have been calculated and plotted individually. An effort has been made to choose the input beam so as to give rise in the total displacements to *distinct features* that can be tied to flaw location and strength. This has led to oblique input beams that generate *resolvable* multiple excursions over the extent of the flaw. The scattered shear waves then become clearly visible on the surface even in the *total* response. Deconvolution techniques for separate extraction of the scattered field displacements can furnish an even more useful data base.

Figures 2-6 contain the numerical data which have been selected for presentation

here. The parameters ːd pertain to an aluminum plate (see Fig. 1):

$$v_p = 2.36 \times 10^5 \text{ in./sec.}, \quad v_s = 1.209 \times 10^5 \text{ in./sec.}$$

$$\rho = 2.53 \times 10^{-4} \text{ lb.} - \text{sec.}^2/\text{in.}^4, \quad a = 0.3 \text{ in.} \tag{9}$$

The flaw length is $2\ell = 0.090$ in., and the shear spring stiffness distribution is assumed to be Gaussian

$$K = K_o e^{[(x-x_f)/\ell]^2}, \quad K_o = 5 \times 10^9 \text{ lb./in.}^3 . \tag{10}$$

The bond location at $z_f = 0.150$in. is midway between the plate boundaries, and the center of the flaw for the four cases considered is located at $x_f = 0.165, 0.135, 0.090, 0.045$ in.
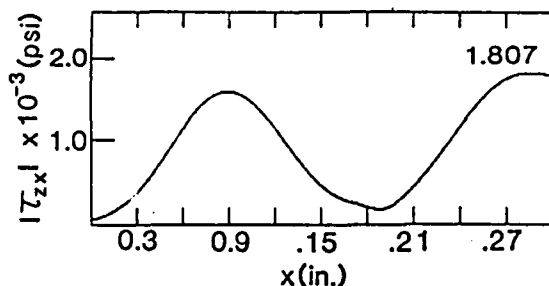

Fig. 2.
Shearing stress generated along bond line of unflawed plate. Note that the first peak corresponds to the incident P-beam and the second peak to the converted SV-beam (see Fig. 1). A number next to a peak denotes the peak amplitude.
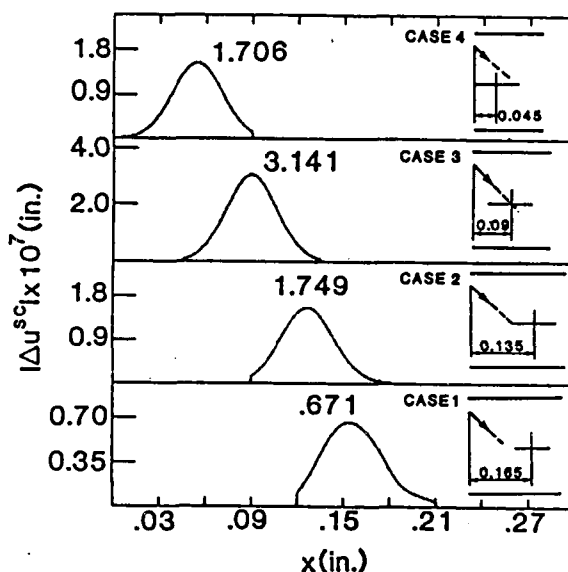
Fig. 3.
Induced source distribution for four flaw locations. Gaussian spring stiffness distribution $K = K_o \exp[(x-x_f)/\ell]^2$, $K_o = 5 \times 10^9$ lb./in.^{3}. Asymmetries in the distribution for Cases 1, 2, 4 arise because the incident beam illumination over the flaw is asymmetrical.

The waist of the 20MHz P-source beam has been placed at $x' = 0.0$ in., $z' = 0.06$in. with beam width parameter $b = 0.3$ in. and corresponding beam waist $w^e = (2b/k_p)^{1/2} = 0.0335$ in. The beam axis inclination angle $\alpha = 45°$ accommodates the resolvability requirement mentioned above, and it also leads to excitation of strong horizontal shear at the flaw site. For these incident beam conditions, there is a cluster of modes (with P-wave congruences surrounding the 45° axis) which contributes appreciably to the shear inducing field on the flaw; only antisymmetric modes need to be included for the calculations because symmetric modes have no horizontal shear at that location. Out of the contributing spectrum of 64 modes (see [2]), a total of 20 (filling the angular spectrum interval $58° \leq \theta \leq 30°$) was retained for the calculations; the error produced by omitting the others is too small to be discerned on the plots. The P-wave angular spectrum spread is compatible with the important spectral content of the incident beam. Spectral filtering tests have been performed to assess the loss of definition when the mode spectrum is truncated further. For example, retaining only 7 modes in the cluster, which fill the angular spectrum interval $38° < \theta < 52°$, one finds a maximum amplitude error of 1% but more significant error in the phase. By choosing a larger beam incidence angle, one may excite a *particular* mode in purer form because the mode separation increases under these conditions. However, this is accompanied by a reduction of the inducing shear, and also by poorer

resolvability of the mu'''ple reflected beams. Such a strate   may be useful for longi-
tudinally extended bo,   with strong imperfections which .an appreciably affect the
mode structure in the flawed interval, thereby making the perturbed mode a good
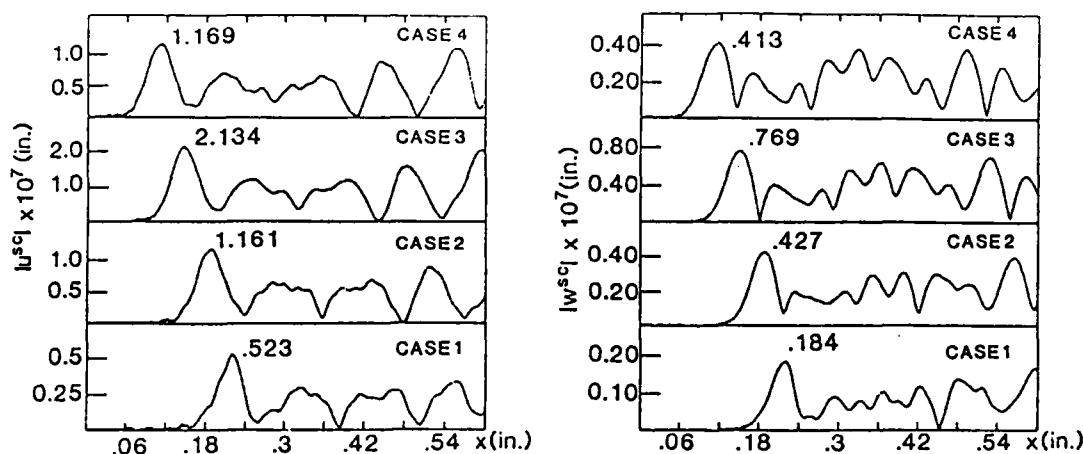observable.

Fig. 4.   Scattered vertical and horizontal displacement fields on upper
               surface of plate. First peaks correspond to intersection of
               direct scattered SV-beam with the surface.

All numerical calculations were performed on a PC/AT compatible Everex 10MHz
System 1800, having a FAST 10MHz 80287 Math Compressor. The scattered dis-
placement fields were determined by evaluating the integrals in (8) numerically, using
30 nodal points (5 to 6 nodes per wavelength) along the flaw. The shearing stress
generated by the input beam along the bond line of the unflawed plate is shown in
Fig. 2. The axes of the incident beam, the reflected P-beam and the converted SV-
beam indicate that the first peak corresponds to the incident P-beam, while the second
peak is associated with the converted SV-beam. For a steeper beam angle α, the hor-
izontal shearing stress due to the P-beam is decreased, rendering the reflected SV con-
tribution dominant. The induced sources along the flaw, computed from (7), are
given in Fig. 3 for the four flaw locations. For Case 3, where the beam axis strikes
the center of the flaw, the induced source magnitudes are largest, and Gaussian sym-
metry is closely maintained. The half-power incident beam width projected onto the
flaw site is 0.05 in.

The scattered displacement fields on the upper surface of the plate are shown in Figs.
4 for the four flaw locations. The scattered shear waves become clearly visible, with
details for Case 3 gleaned from Fig. 5. Note that the first peak occurs at the intersec-
tion of the direct scattered SV-beam and the surface, and that the shape about that
peak has similarities with the shape of the induced source distribution. Subsequent
peaks line up with the multiple reflected SV-beams.

The displacements on the surface generated by the input beam in the plate, by the
scattering from the flaw, and by the combination of both have been plotted individu-
ally in Fig. 6 for Case 3. Clearly visible in a region which was initially quiescent is the
disturbance attributable to the scatterer. The corresponding real displacement com-
ponents are also shown. The observed periodicities turn out to be essentially those
found in the guided mode whose upgoing reflected plane wave SV-spectra line up best
with the dominant wave spectra of the incident P-beam; the amplitude modulation is
due to interference between several of the modes in the surrounding cluster. The
small oscillatory precursor in the total displacements, which appears to the left of the
undisturbed region in the unflawed plate response, is explicitly tied to the flawed
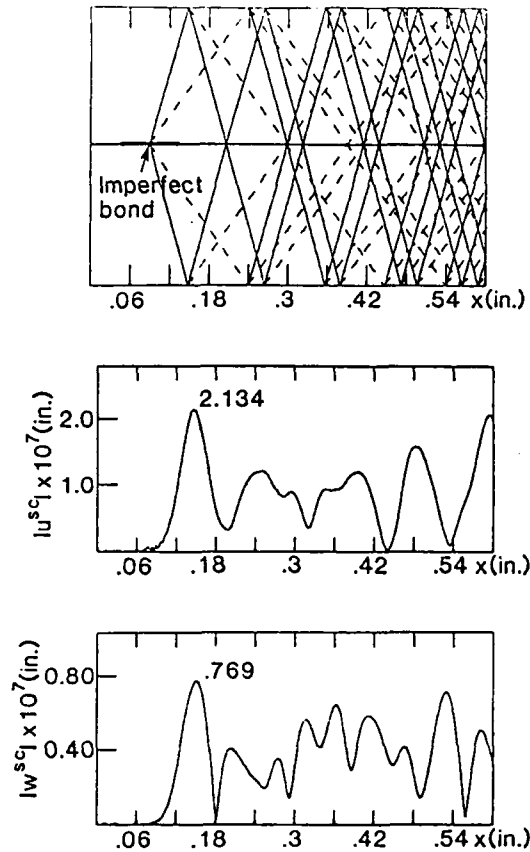environment.

Fig. 5.
Enlarged scattered displacement fields for Case 3 of Fig. 4, and associated beam axis trajectories. Incident and reflected P-beams: dashed lines; coupled SV-beams: solid lines. Prominent features in the displacements are seen to occur near the beam axis intersections.
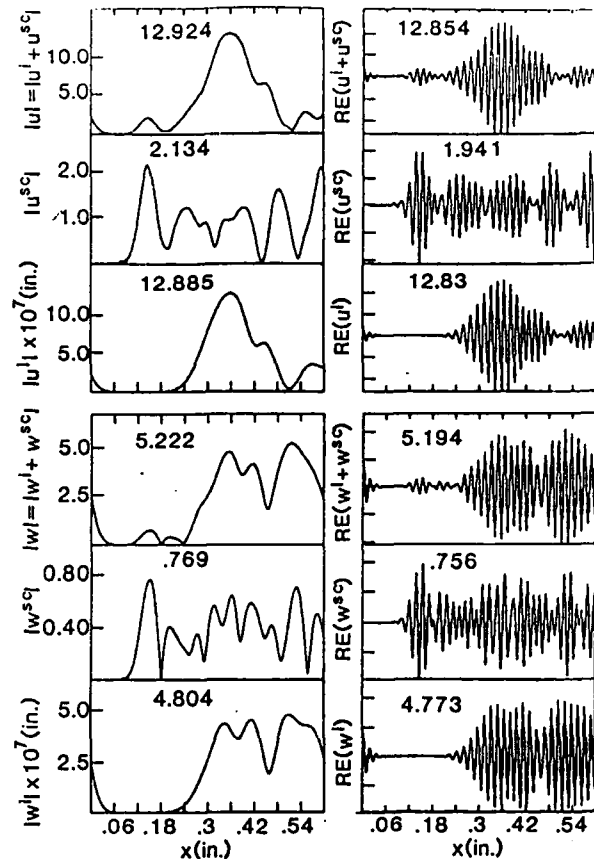
Fig. 6.
Displacements on plate surface for Case 3 of Fig. 4. $|u^i|$, $|w^i|$: generated by input beam. $|u^{sc}|$, $|w^{sc}|$: generated by scattering from flaw. $|u| = |u^i + u^{sc}|$, $|w| = |w^i + w^{sc}|$: combination of both. Also shown are the corresponding real displacement components; the imaginary components (not shown) exhibit similar characteristics. Phase plots (not shown) possess essentially the linear variation associated with the P-excited incident SV-plane wave observed at the boundary, except near the onset of the first disturbance where the field departs strongly from the plane wave prototype.

To link the measured displacements on the surface with the flaw that induces the perturbations, we are continuing the search for other observables, in addition to those described above. There are indications that the readily accessible ratio (u/w) contains information which can be related to the flaw location by simple ray construction, while inferences on flaw strength can be drawn from the data for u or w individually. Details of the inversion process, i.e., specifying flaw parameters from measured displacements at the surface, are still under investigation and will be reported separately.

5. SUMMARY

This study has been directed toward a "good parametrization" of observables when a Gaussian P-beam input in a perfectly bonded layered two-dimensional elastic plate encounters a transversely thin region with weak debonding of shearing stress. The

observables are the horizontal and vertical displacements on the surface of the plate; the parametrization seeks to connect these observables with presence, location, and physical constitution of the flawed region. Emphasis here has been on how the plate environment, first without and then with the flaw, affects the incident beam; i.e., the parametrization is beam oriented. In this endeavor, the choice of input conditions that combines multiple beam resolution with strong shear excitation at the site of the flaw plays a critical role. The numerical results have shown that a good parametrization can be achieved. Some indications have been given on how to make the inverse connection between surface displacements and flaw identification but work on this aspect is still in progress.

Despite the beam oriented parametrization, the results have been computed by mode summation because the complex-source-point adapted mode algorithm has been available from a prior phase in this investigation [2]. Evidently, the numerical algorithm should be restructured in hybrid beam-mode form [2,5,6] to highlight the parametrized observables directly. Consideration of this aspect is postponed until a thorough understanding has been gained of the variety of phenomena that accompany the flaw identification problem in a multilayer bonded plate environment.

ACKNOWLEDGMENTS

REFERENCES

[1] Felsen, L.B., "Geometrical Theory of Diffraction, Evanescent Waves, Complex Rays and Gaussian Beams," Geophys. J. Roy. Astron. Soc., 79, 77-88 (1984).

[2] Lu, I.T., Felsen, L.B., and Klosner, J.M., "Beam-To-Mode Conversion of a High Frequency Gaussian P-Wave Input in an Aluminum Plate in Vacuum," to be printed in ASME *Symposium on New Directions in the Ultrasonic NDE of Advanced Materials.*

[3] Pao, Y-H. and Varatharajulu, "Huygens' Principle, Radiation Conditions, and Integral Formulas for the Scattering of Elastic Waves," J. Acoust. Soc. Am., 59 (6), 1361-1371 (1976).

[4] Morse, P.M. and Feshbach, H., *Methods of Mathematical Physics* (McGraw Hill, N.Y. 1953).

[5] Lu, I.T. and Felsen, L.B., "Matrix Green's Functions for Array-Type Sources and Receivers in Multiwave Layered Media," Geophys. J. Roy. Astron., Soc., 84, 31-48 (1986).

[6] Lu, I.T. and Felsen, L.B., "Ray, Mode, and Hybrid Options for Source Excited Propagation in an Elastic Plate," J. Acoust. Soc. Am. 78 (2), 701-714 (1985).

ATE
LMED
8